Advanced Energy Conversion Materials
https://ojs.wiserpub.com/index.php/AECM/

UNIVERSAL WISER PUBLISHER

Research Article

Growth of the Electrodeposited NiX_2 (X = Te, Se) Thin Films

T. Joseph Sahaya Anand[1*], Rajes K. M. Rajan[1], Md Radzai Said[2], Lau Kok Tee[3]

[1]Faculty of Manufacturing Engineering, Technical University of Malaysia Malacca, Malaysia
[2]Faculty of Mechanical Engineering, Technical University of Malaysia Malacca, Malaysia
[3]Faculty of Technology Engineering, Technical University of Malaysia Malacca, Malaysia
E-mail: anand@utem.edu.my

Received: 31 December 2019; **Revised:** 22 April 2020; **Accepted:** 25 April 2020

Abstract: Thin films of nickel chalcogenide, NiX_2 (X = Te, Se) have been electrosynthesized on indium-tin-oxide (ITO) coated glass substrates. The films were characterized for their structural, morphological and compositional characteristics. Consisting of transition metals and chalcogenides (S, Se and Te), they show promising solar absorbent properties such as semiconducting band gap, well adhesion to substrate and good conversion with better cost-effective. Cyclic voltammetry experiments have been done prior to electrodeposition in order to get the electrodeposition potential range where the observable reduction range is between -0.9-(-1.1) V. Their optical and semiconducting parameters were also analysed in order to determine the suitability of the thin films for photoelectrochemical (PEC)/solar cell applications. Structural analysis via X-ray diffraction (XRD) analysis reveals that the films are polycrystalline in nature. Scanning electron microscope (SEM) studies reveals that the films were adherent to the substrate with uniform and pin-hole free. Compositional analysis via energy dispersive X-ray (EDX) technique confirms the presence of Ni, Te, and Se elements in the films. The optical studies show that the films are of direct bandgap. Results on the semiconductor parameters analysis of the films showed that the nature of the Mott-Schottky plots indicates that the films obtained are of p-type material.

***Keywords*:** chalcogenides, thin films, electrochemical techniques, optical properties

1. Introduction

Growing fuel prices and fast depleting conventional energy source has led to findings on sustainable and efficient energy source. Hence, renewable energy has been suggested as a viable approach for this particular energy crisis. Presently, many research group has focused on solar energy as the most promising renewable energy to cater the future energy demand due to its abundance and inexhaustibility [1]. The well-known silicon solar cells made, either amorphous or polycrystalline are good in conversion efficiency up to 17%, but their high cost make the researchers to look for alternate materials. Semiconducting materials in thin film form such as InP, SnO_2 and ZnO are being studied as the alternative materials, but are not commercialised due to their poor conversion efficiency. Another group of semiconductor compounds known as transition metal chalcogenides (TMC) have been developed to be used as the absorbent materials [2]. Consisting of transition metals and chalcogenides (S, Se and Te), they show promising solar absorbent properties such as semiconducting band gap, well adhesion to substrate and good conversion with better cost-

DOI: https://doi.org/10.37256/aecm.112020191

effective. There are many TMC compounds synthesised, including copper indium selenide (CIS).

Photoelectrochemical (PEC) cell is a solar device which is fabricated with semiconductor electrolyte interface for solar energy conversion into electrical energy. Being an advance microelectronic technology, PEC can be applied for both photo voltage and chemical energy conversion [3]. At present, silicon material is widely used for PEC fabrication. However, silicon is extremely expensive for large scale production [4]. Thus, research is being carried out extensively in finding new materials for energy conversion for reasonable cost without compromising their conversion efficiency [5].

Thin films referred as transition metal chalcogenides (TMC) have alternatively been used as the absorbent material for solar cells to replace the widely used silicon. Though many thin films of oxides, tellurides and selenides have been synthesised, few studies of telluride thin films such as Bi_2Te_3, $Hg_{1-x}Cd_xTe$, CdTe, CoTe and Ag_2Te have been reported [6]. As one of the transition metal chalcogenides, nickel chalcogenides, NiX has been deposited in the form of thin film onto indium tin oxide (ITO)-coated glass substrates to be further developed into thin film solar cell. Though there is no reported literature about the use of NiX_2 to function as a solar cell, this material has the high potential to be the candidate materials of solar cell. The syntheses of telluride thin films involve several techniques such as physical vapour deposition (PVD), metal organic vapour chemical deposition (MOCVD), solvothermal methods, coreduction method (in- situ), and electrodeposition [6]. The PVD technique is excellent for good quality film growth but is difficult to scale up [7]. The absorber layers for high-quality devices are typically synthesised via high vacuum deposition processes such as co-evaporation that is costly due to initial cost of equipment and production of vacuum [5]. Therefore, there is great interest in developing non-vacuum, large scale and low-cost technique such as electrodeposition [3] for preparing NiX thin films. Owing to this effort in finding new materials, Transition Metal Chalcogenides (TMC) are proposed as the most satisfactory semiconductor materials for PEC application. TMC, a combinatorial of transition metal (group 10) and chalcogenide (group 16), MX_2 (M: Cd, Mo, Zn, etc.; X: S, Se and Te). TMC possesses excellent optical, electrical and semiconductor properties, especially in the thin film form [6]. This advancement has motivated many researchers to investigate TMC thin film materials for PEC application namely, CdS [7], CdSe [8], ZnS [9], SnS [10] etc. Cadmium chalcogenides are the most widely used TMC material for energy conversion purpose due to its significant photo conversion efficiency [8, 11]. However, in a recent study, Nickel has been expected to substitute Cadmium in thin film chalcogenide as a material with better electrical properties to meet solar cell expectations. It is reported that, Ni^{2+} has a standard ionic radius of 0.069 nm, which is less than Cd^{2+} (0.097 nm) and higher electronegativity of 1.91 Pauling compared to Cd^{2+} (1.61 Pauling) [12]. Hence, with smaller ionic radius, nickel chalcogenides could form stronger ionic bonds with higher electronegativity that makes it attract electrons effectively. Chalcogenides thin films can be fabricated by spray pyrolysis [3], electrochemical deposition [13], sputtering [14] etc. One of the attractive methods for producing nickel chalcogenide thin film, owing to the possibility of large area deposition at low cost is the electrodeposition method. This method requires presence of reagents that act as a source of chalcogenide and complexion of metal ions that forms via 'ion-by-ion growth' mechanism [6].

The first report on these nickel chalcogenides was published by Biswas in 1986 [15]. The results obtained shown that these chalcogenides are close to metallic behaviour due to the influence of nickel. After about two decades researchers started again on these materials but mostly focussed on chemical methods [16-18]. As it is shown that nickel chalcogenides have higher electronegativity, it is proposed to study their synthesis, growth mechanism, optical and semiconducting properties of these thin films in a more systematic way. Selenium is a metal chalcogens and non-metal (X = Te, Se) while Tellurium (Te) is a metalloid.

2. Experimental details

2.1 *Preparation of thin film substrates and electrolytes*

All reagents used for the deposition were of analytical grade. Prior to the deposition, the Indium Tin Oxide (ITO) coated glass substrates were ultrasonically cleaned in deionized water and followed by ethanol. All solutions were prepared using 30 mL of deionized water. The electrodeposition of thin film semiconductors on ITO-coated glass substrates was carried out at 40 ± 1 °C of temperature in an aqueous solution containing Nickel Sulphate Hexahydrate, $NiSO_4 \cdot 6H_2O$ (1 mM) + Sodium Thiosulphate Pentahydrate, $Na_2S_2O_3$ (3 mM) + Tellurium dioxide as precursors for Nickel Telluride ($NiTe_2$) solution. Solution for $NiSe_2$ were also prepared in the same manner except of Sodium

Selenide Na_2SeO_3 (4 mM) was used instead of $Na_2S_2O_3$. Triethanolamine (TEA) (0.1 M) has been added as an additive into the bath solution for successful film adhesion on the ITO-coated glass substrate [19]. Besides adhesion, TEA also helps to deposit uniform and thicker deposition by controlling the deposition rate of the metal ions [19]. pH of the solution was adjusted to ~ 10 by adding NaOH (2.5 mM) drop by drop [6] for uniform deposition.

2.2 *Characterization of electrodeposited NiX_2 thin films*

The electrochemical experiments, including cyclic-voltammetry (CV) and electrodeposition were controlled by Princeton Applied Research Model VersaSTAT 3 Potentiostat in a three-electrode cell, which consist of ITO-coated glass substrate as the working electrode (WE), graphite as counter electrode (CE) and Saturated Calomel Electrode (SCE) as the reference electrode (RE) as described in [6]. All the three electrodes kept as close to each other with the optimum distance of 1 cm for uniform deposition [20]. Film thickness of NiX_2 (X = Te, Se) was determined by gravimetric weight difference method using sensitive microbalance and assuming film density as close to the bulk density of the compounds [20]. X-ray diffraction (XRD) and scanning election microscopy (SEM) analysis were carried out in PANalytical ZPERT PROMPD PW 3040/60 diffractometer (for 2θ range from 20 to 70° with CuKα radiation) and SEM ZEIZZ EVO 50 scanning microscope, respectively and its composition analysis with energy dispersive X-ray (EDX) analysis. Optical properties for determination of energy band gap of the films and semiconductor properties of the films studied using UV-Vis spectrophotometer and Mott-Schottky plot analysis, respectively. Mott-Schottky plots were plotted using a LCR (ZENTECH 1075-LCR at built-in frequency of 1 kHz) by adopting a two electrode configuration consisting of the thin film photo electrode and graphite as the counter electrode as illustrated in [21].

2.3 *Cyclic voltammetry*

Cyclic voltammetry (CV) is a powerful electro analytical tool for finding redox couples and confirming the electrode potential during the film deposition process [22]. Figure 1 depicts the cyclic voltammetry of $NiSO_4 + Na_2Te_2O_3$ and $NiSO_4 + Na_2Se_2O_3$ solution bath.

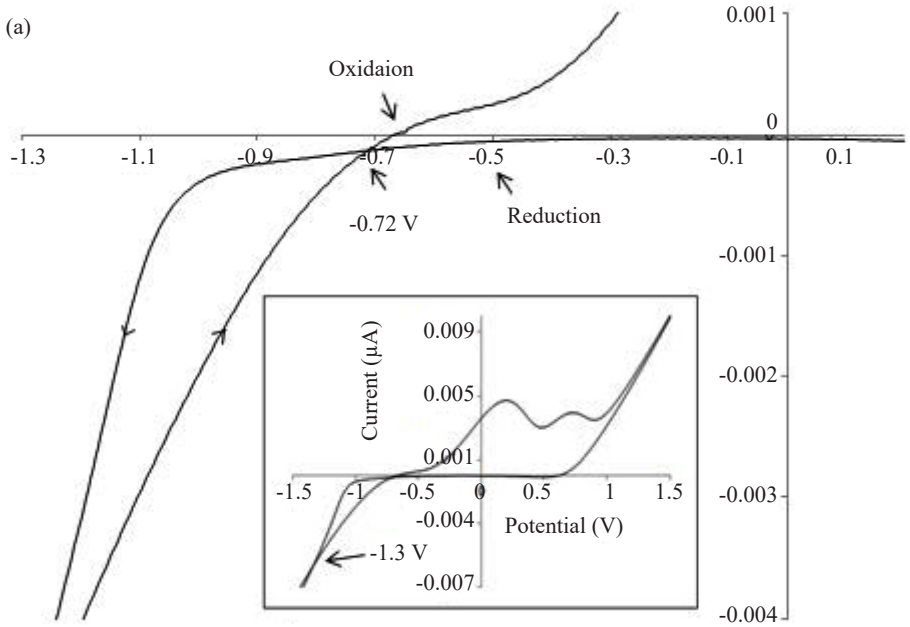

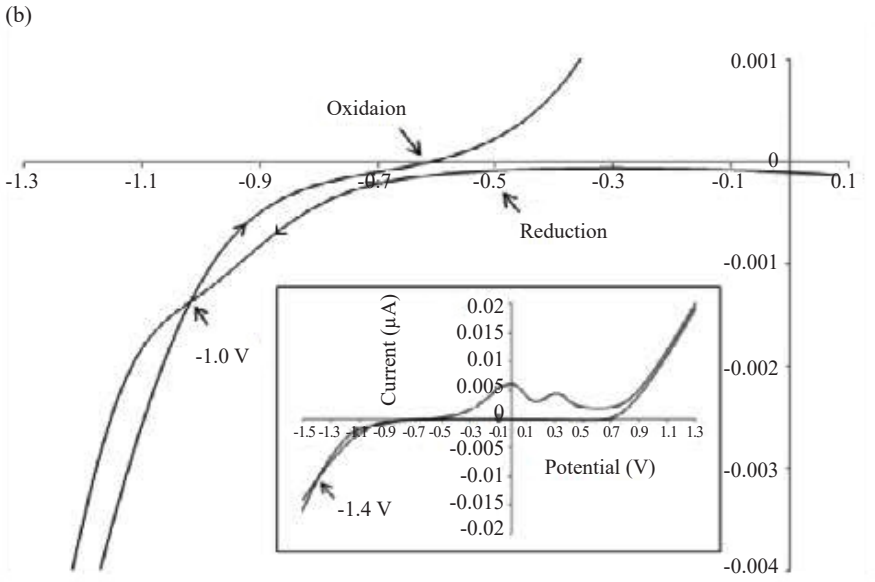

Figure 1. Cyclic voltammogram of the electrodes using ITO-coated glass substrates in alkaline solution bath of TEA and (a) $NiSO_4 + Na_2Te_2O_3$ (b) $NiSO_4 + Na_2Se_2O_3$

From Figure 1 it is observed that current rise in forward scan of both $NiSO_4 + Na_2Te_2O_3$ and $NiSO_4 + Na_2Se_2O_3$ solution bath occurs approximately at -0.5 V followed by two large anodic peaks. Anodic peaks correspond to oxidation of nickel compound which generally emerge at positive potential region [23]. As for $NiSO_4 + Na_2Te_2O_3$ solution (Figure 1a), the interception between forward and reverse scan observed at -0.72 V and achieved another interception at -1.30 V. However, $NiSO_4 + Na_2Te_2O_3$ solution (Figure 1b), the first interception observed at -1.0 V and the second interception at -1.4 V. Interception of forward and reverse scan is an important phenomenon in a cyclic voltammetry due the fact, interception confirms the deposition reaction in the latter solution until all equiblirium potential is achived and completes with second interception [24]. In specific, co-deposition of nickel compound occurs at this particular region. The high current output during the reduction process indicates that the presence of TEA increases the rate of deposition. Further current rise at more negative potential was due to hydrogen evolution. It is important to mention that, no stripping peaks were available in the reduction region. It coincides, nickel compound formed on the surface of the substrate does not dissolve completely into the solution containing TEA during the reverse scan [24]. From Figure 1, both NiX (X = Te, Se) chalcogen observed to have similar trend of cyclic voltammetry. It could be due to the applied chalcogen (Te, Se) which likely have similar chemical behaviors and reactions.

3. Results and discussion

3.1 *Kinetics and growth mechanism*

Thin film formation of NiX_2 (X = Te, Se) occurs as the result of various chemical reactions taking place in the deposition bath are possibly summarized as follows: (a) the ions diffuse to the electrode surface in the electrolyte; (b) adsorbed ions are reduced at the cathode; (c) nickel, sulphide, selenium ions migrate to the reduction reaction zone and produce binary compound semiconductors [22] which initiates 'ion-by-ion' growth. In the present investigation, ionic species of nickel, telluride and selenide are produced by the following reaction equilibria in an aqueous alkaline deposition bath.

(i) Nickel oxidation:

$$NiSO_4 \cdot 6H_2O \rightarrow H_2SO_4 + NiO + 5H_2O$$

$$NiO + 2H^+ \rightarrow Ni^{2+} + H_2O \quad (1)$$

(ii) Chalcogenide reduction:

$$Na_2Te_2O_3 \cdot 5H_2O + e^- \leftrightarrow Na^+ + Te_2O_3^{2-} + NaOH + 4H_2O$$

On the substrate surface, $S_2O_3^{2-}$ reduces to telluride:

$$Te_2O_3^{2-} + 6H^+ + 6e^- \rightarrow 2Te^{2-} + 3H_2O$$

$$Na_2SeO_3 + e^- \leftrightarrow Na^+ + SeO_3^{2-} \quad (2)$$

On the substrate surface, SeO_3^{2-} reduces to selenide:

$$SeO_3^{2-} + 6H^+ + 6e^- \rightarrow Se^{2-} + 3H_2O \quad (3)$$

Reaction (1) shows that metal ions are produces by dissociation of the metal complex while chalcogenide ions (Reaction (2) and (3)) are produced by dissociation of sulphur and selenium precursors in the aqueous alkaline medium. When the concentration of ionic species Ni^{2+}, Te^{2-} and Se^{2-} exceeds in the reaction bath, nucleation starts which results in growth of these thin films. The as-reduced Ni, Te, and Se atoms are very active and can easily combine to produce NiX_2 compound. The kinetic growth of film can be understood from the following:

(i) $NiTe_2$ formation:

$$Ni^{2+} + 2Te^{2-} \rightarrow NiTe_2 \text{ (Nickel Telluride)}$$

(ii) $NiSe_2$ formation:

$$Ni^{2+} + 2Se^{2-} \rightarrow NiSe_2 \text{ (Nickel Selenide)}$$

The growth of the film was studied through the film thickness plot as shown in Figure 2. It shows an initial induction period about 10 min and thereafter, the film begins to grow. The initial induction time in the electrolyte bath is necessary for the nucleation to start on the ITO conductive glass substrate. This confirms the 'ion-by-ion' growth mechanism where nucleation occurs first and act as a catalyst followed by the combination of ions for the subsequent layer of thin film growth [15].

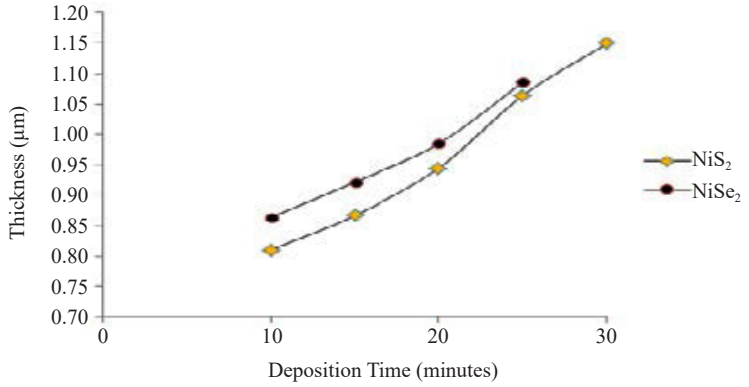

Figure 2. Variation of thickness with deposition time for $NiTe_2$ and $NiSe_2$ thin films deposited on ITO-glass substrate

As for 10 minutes of deposition time, the film thickness rapidly increases in the range of 0.81-0.87 μm in NiX_2 (X = Te, Se) films. Dhanasekaran et al. has claimed that when a temperature (45 °C) is applied to a solution there would be more ions available compared to room temperature [25]. It is important to study that a fixed temperature of 40 ± 2 °C is applied to the solution for the influence during the deposition. Temperature plays an important role in increasing the precursor solubility and increasing the diffusion coefficient of the species and decreasing the viscosity. Thus, as soon as the deposition is started, the film thickness increases with more ions availability. Hence, it is possible for the film thickness to increase rapidly during the induction time and thereafter the thickness increase gradually as the ion diffusion become stable at constant 40 ± 2 °C throughout the deposition process. For the few cyclic voltammogram carried out it is found that As for NiS_2 film, based on the CV range the deposition started to occur at -0.8 V at 15 minutes and the films display mostly amorphous nature. Improved crystallinity and film uniformity was observed at film prepared at -0.9 V. However, film cracked and peeled off from ITO-coated substrate at -1.0 V, 20 minutes. On the other hand, $NiSe_2$ film growth was observed at -0.8 V at 30 minutes and continued at -0.9 V. Films prepared at these potentials result poorer crystallinity with less adhesion on the ITO-coated substrate. But, at -1.0 V, films possess improved characterization properties. Thus, it can be understood that film distribution with good uniformity and well crystalline at potential -0.9 V for NiS_2 film and -1.0 V for $NiSe_2$ film was obtained.

Films were found to be well covered; with $NiTe_2$ films were in dark greyish color while $NiSe_2$ films were in dark red as observed by the optical microscope. Film thickness increases linearly with deposition time tend to attain its maximum value at deposition time of 30 min and 25 min for $NiTe_2$ and $NiSe_2$, respectively. There is a distinct increase in thickness of the both $NiTe_2$ film about 12% and $NiSe_2$ 10% at 25 minutes. This is close to the general trend of Se, Te chalcogens thin films thickness measurement [26]. It is also observed from the literature, when the film thickness exceeded the optimum value, the layers started to peel off from the substrate [27]. This has been confirmed in the present investigation that, NiS_2 film started to peel off from the substrate at deposition time of 35 minutes and $NiSe_2$ peeled off at 30 minutes.

3.2 *Structural characterization*

Figures 3 and 4 show the XRD patterns of both $NiTe_2$ and $NiSe_2$ film. All standard and experimental '*d*' spacing values with reference to JCPDS cards are summarized in Table 1. This XRD analysis was performed at incident angle of 1.5° to reduce intensity of radiation reflected by the ITO glass substrate [28]. It should be noted that metal substrate was not employed in this investigation corresponding to the presence of nickel which is normally detected by the metal substrate's chemical composition. Consequently, it may lead to non-stoichiometry result in analysing NiX_2 (X = Te, Se) films. Undoubtedly, it is important to differentiate the XRD peaks of the substrate and the films to characterize their crystalline structure.

Peaks belonging to $NiTe_2$ film deposited for a period of 10-30 minutes is detected and labelled as shown in Figure 3. The structural features fit into the cubic structure of the $NiTe_2$ film with lattice parameter values $a = b = c = 5.668$ nm which is in good agreement with the standard values [29]. Only a single peak is attributable to NiS with lattice plane (2 2 0) at $2\theta = 45.5°$. Intensity of the peak (2 2 0) increases dramatically at 30 minutes indicating that the film grow with respect to time. From Figure 3 it is clear that the intensity of ITO peaks are initially higher for 10 minutes film which is further suppressed as the deposition time increases. This is confirmed that higher film thickness reduces the effect of substrates it utilized.

Figure 4 shows the XRD patterns of $NiSe_2$ films and peaks emerged at $2\theta = 47.48°$ and 55.73° that identified as (2 2 1) and (1 3 1) plane, respectively. The structural features fit into orthorombic structure of the $NiSe_2$ films with lattice parameter values $a = 4.89$, $b = 5.96$, $c = 3.96$ nm which is in good agreement with the standard values [30]. At 20 minutes, *hkl* plane (1 3 1) started to emerge more definably that could be resulting from effective mass transfer forms a thicker film as the deposition time increases. Intensity of the plane (2 2 1) found to be more prominent than plane (1 3 1) which indicating (2 2 1) peak is the preferred orientation. However, the intensity of (2 2 1) and (1 3 1) plane shrinked at 30 minutes deposition time due to crystallinity deterioration. Crystallinity deteriorates at longer deposition time causing film to break and peel off.

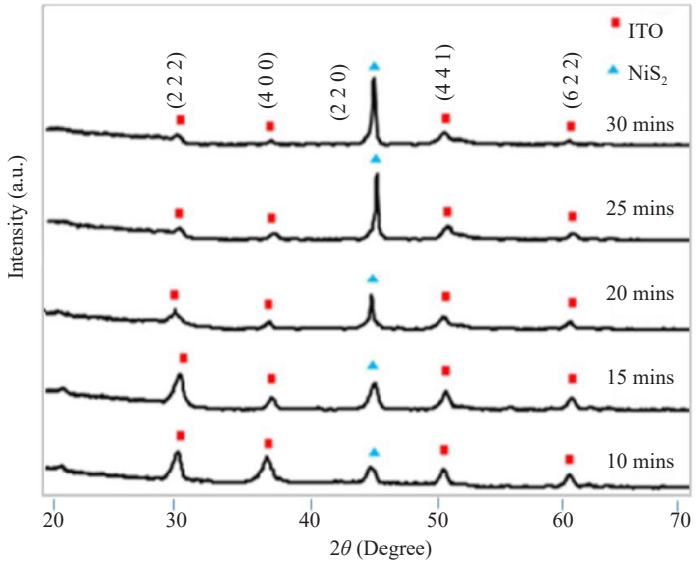

Figure 3. XRD pattern for $NiTe_2$ thin films deposited on ITO glass substrate at different deposition times

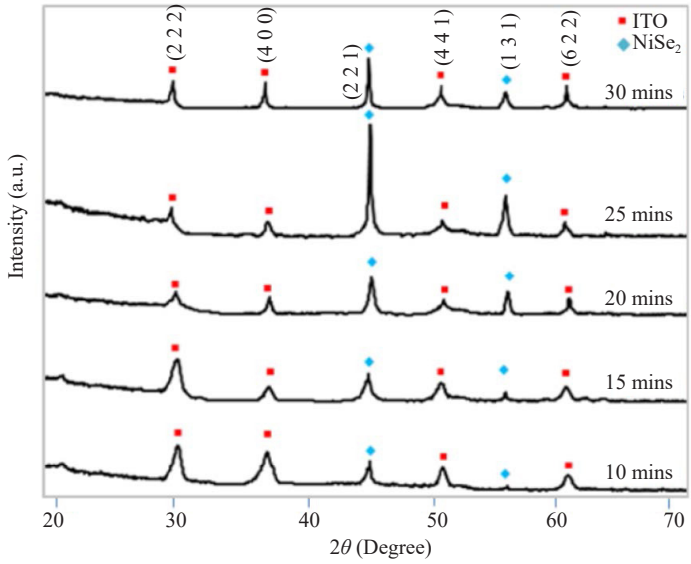

Figure 4. XRD pattern for $NiSe_2$ thin films deposited on ITO glass substrates at different deposition times

Table 1. Comparison of experimental '*d*' values with JCPDS data for NiX_2 (X = Te, Se) thin film

Material	Structure	Angle (2θ)	Planes ($h\ k\ l$)	Standard ($\acute{A}$)	Experimental ($\acute{A}$)				
				'*d*' JCPDS	10 min	15 min	20 min	25 min	30 min
$NiTe_2$	Cubic	45.547	2 2 0	1.9900	1.9733	1.9544	1.9216	1.8461	1.7436
$NiSe_2$	Orthorhombic	47.176	2 2 1	1.9250	1.9011	1.8772	1.8008	1.7745	1.9843
		55.733	1 3 1	1.6480	1.6302	1.6321	1.6201	1.5984	1.6272

According to the Debye-Scherer approach [25], the interplanar distance '*d*' corresponding to different (*h k l*) planes that calculated from the X-ray diffractograms. The crystallite size was calculated from the measurement of full-width at half-maximum (FWHM) in different X-ray peaks and values are in the range of 38-60 nm for NiS_2 and 15-35 nm for $NiSe_2$ which is in similar trend observed for other TMCs [31].

From Figures 3 and 4, it is understand that the NiX_2 (X = Te, Se) has formed pure NiS_2 and $NiSe_2$ film without other phases and elements such as Ni, Ni_3S_2, NiSe or other intermediary phase of both NiS_2 and $NiSe_2$ formed. The sharp and more intense diffraction peaks of these films reveals the formation of films with improved crystallinity [20]. It is important to remark that, enhancement of film crystallinity achieved due to increase of film thickness and strain decrease along with increase in grain size from the polycrystalline nature of films [32]. As mentioned earlier, deposition time has influence on NiX_2 (X = Te, Se) thin film growth since structure and grain growth of the film is mainly dependent on reaction (deposition) kinetics.

Higher deposition time shows that the decrease of the lattice constant, '*d*' which confirms the improved crystallinity as shown in Table 1. This attributed due to decrease of Full Width Half Maximum (FWHM) with narrowing of the lines of crystal growth which indicates the grain size has increased. Contradically, the increase of the lattice constant indicates the film peel off from substrate for films deposited more than 30 minutes. Hence, the crystallinity improvement or deterioration of the film peaks can be confirmed through the changes in lattice spacing and their corresponding lattice parameters [33].

3.3 *Morphological characterization of NiX_2 thin films*

The surface morphology of the NiX_2 (X = Te, Se) films obtained with different deposition times are shown in Figures. 5 and 6. The deposited films were confirmed homogenous, well adherent to the substrate and uniform with the use of electron microscope. From the planar SEM of the films were investigated, it clearly shown that as the deposition time increases, the size of the crystallites and the number of aggregations in the films increased, resulting more homogeneous structure. Slow nucleation and growth rate at lower deposition time (10 minutes) causes incomplete growth in the film as it is also supported by previous XRD analysis. Thereafter, sufficient deposition time is necessary for deposition kinetics to take place in the reduction bath.

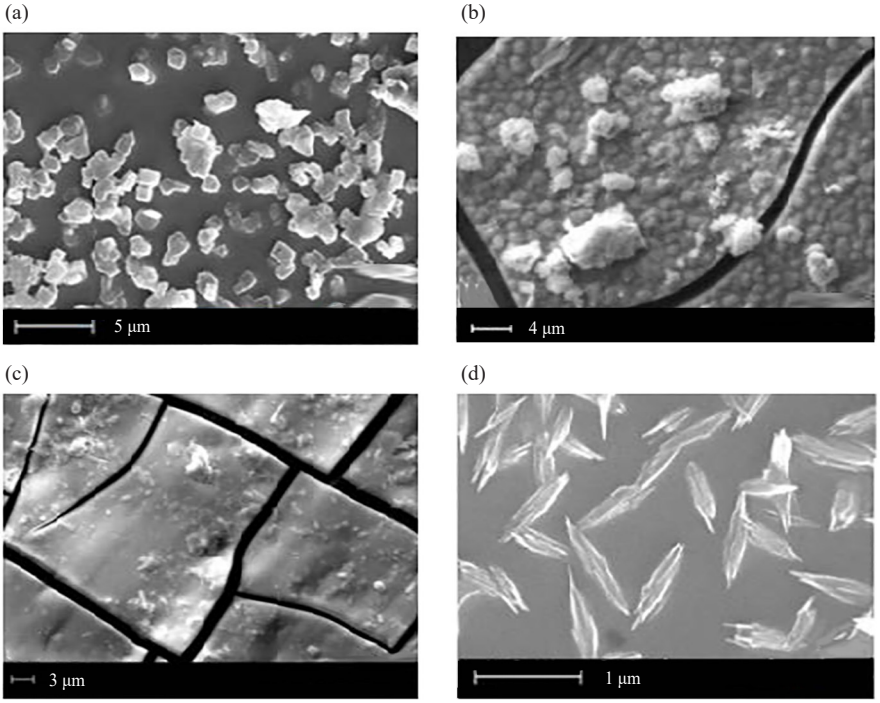

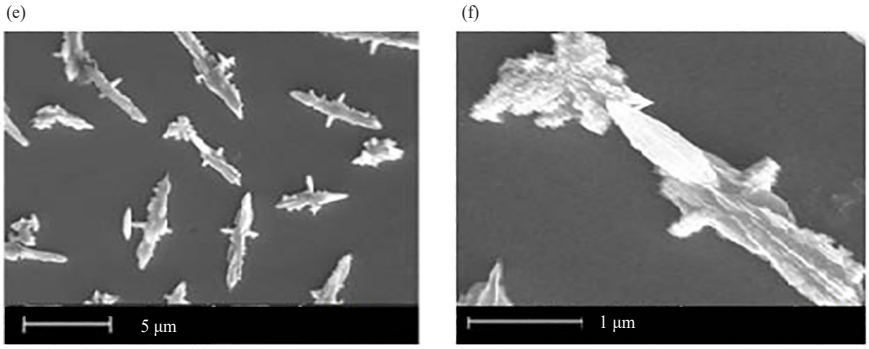

Figure 5. Planar SEM of $NiTe_2$ (a) 10 min (1,000 ×) (b) 10 min (5,000 ×) (c) 20 min (1000 ×) (d) (5,000 ×) (e) 30 min (1,000 ×) (f) (5,000 ×)

Figure 5 shows the morphology of $NiTe_2$ film prepared for 10, 20 and 30 minutes. The formed platelet grains at the beginning of the film growth is disappeared and transformed into needle structure as the deposition time increases. At 20 minutes, a platelet grain is found among needle structures. It may be attributed to rearrangement of the film structure caused by effective mass transfer and indicating the film growth is incomplete [34]. Films found to be completely in needle structure, homogeneous, smooth and evenly distributed at deposition time of 30 minutes. Additionally, number of aggregations in the film found to have increased due to denser film at the latter deposition time [35]. Similar observation of that needle like crystallites provide direct pathway for the transport of the photogenerated carriers and mobility of carriers in such microstructure is higher resultant of less number of intergrain boundaries [34]. The variation of the calculated average platelet grain size is in the range of 0.61-0.70 µm. However, the needle like grains are in the average length of 2.72-4.36 µm and diameter of 0.12-1.23 µm.

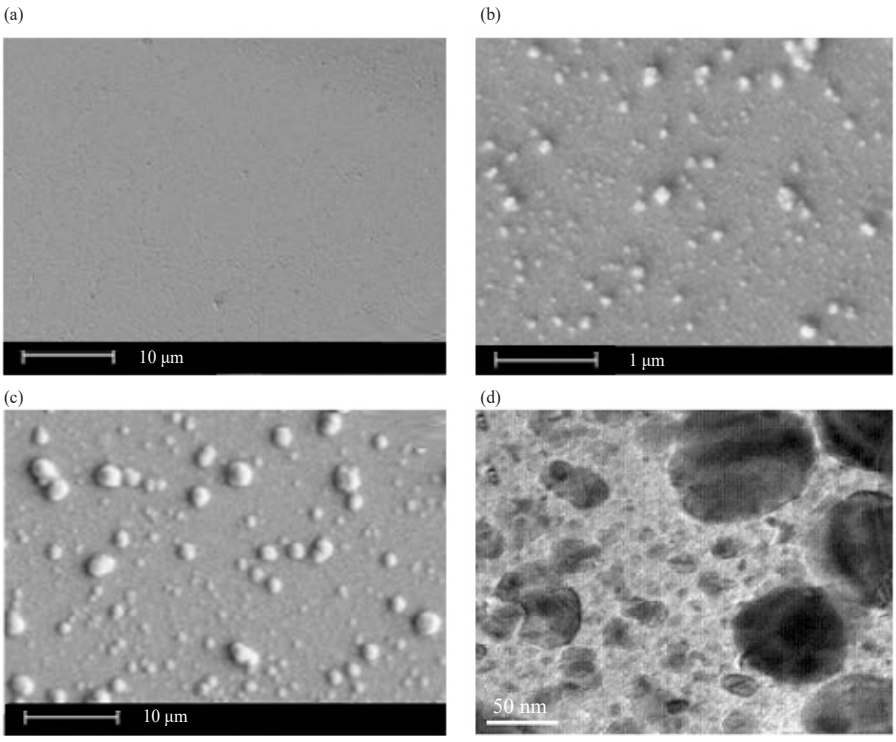

Figure 6. Planar SEM of $NiSe_2$ (a) 10 min (1,000 ×) (b) 10 min (5,000 ×) (c) 25 min (1,000 ×) (d) (50,000 ×)

On the other hand, the morphology of the $NiSe_2$ film is found to be well defined in spherical shape in Figure 6. Few

crystallites are grouped together forming larger grains. It could be of the effect of Ostwald ripening process as Se elemental is reported to have amorphous structure in alkaline bath and often aggregates to form spherical morphology [36]. The calculated grain size found to be in the range of 0.12-0.39 μm. Additionally, the films are found to be continuous, well covered, homogenous and without voids up to 25 minutes, thereafter, film started to crack and peel off. Longer deposition time primely bring the effect of the growth of the particles with constant temperature [37]. This explains that longer the deposition time does not promise better film morphology. As the size of the grains increase corresponding with increasing deposition time, the film become thicker and strain energy increases. Consequently, the film cracks to release the stress accumulated [38].

It is observed that, the morphology of the structure is smoother for films with sulphur content as compared to its $NiSe_2$ counterpart. Theoretical calculation of grain size is slightly varied with the actual experimental morphology as the grain growth is influenced by preparation method and its parameters. It should be noted that, all grain size of the film is larger than 1 μm. Chui et al. claims that larger grain size (> 1 μm) could increase energy conversion of solar cell of an absorber material [39]. Hence, the prepared NiX_2 (X = Te, Se) thin films can be considered as one of the suitable materials for the application in solar cell.

3.4 *Compositional characterization by EDX analysis*

As shown in Figure 7, Energy Dispersive X-ray (EDX) was used to analyse the film stoichiometry of the prepared samples of 30 and 25 minutes for NiS_2 and $NiSe_2$ respectively. These samples are considered to be the optimum films for revealing their stoichiometry. The strong peaks in the spectra for Ni, Te, and Se were identified and are near stoichiometric with ratio close to 1 : 2 as presented in Table 2. Although elements of C and O do not have any influential role in the synthesis of the films, their peaks also observed in the spectrum corresponding to the capability of EDX to detect as low atomic number elements such as carbon and oxygen, which is ubiquitous in our environment. Inclusion of oxygen is found in all the films because it is found to be unavoidable for chemically deposited films as testified. This is true and accepted for all films synthesized [6]. Furthermore, the spectrums also display smaller peaks of Na, which has been expected as Na was used as a precursor in the electrolyte for the deposition of films.

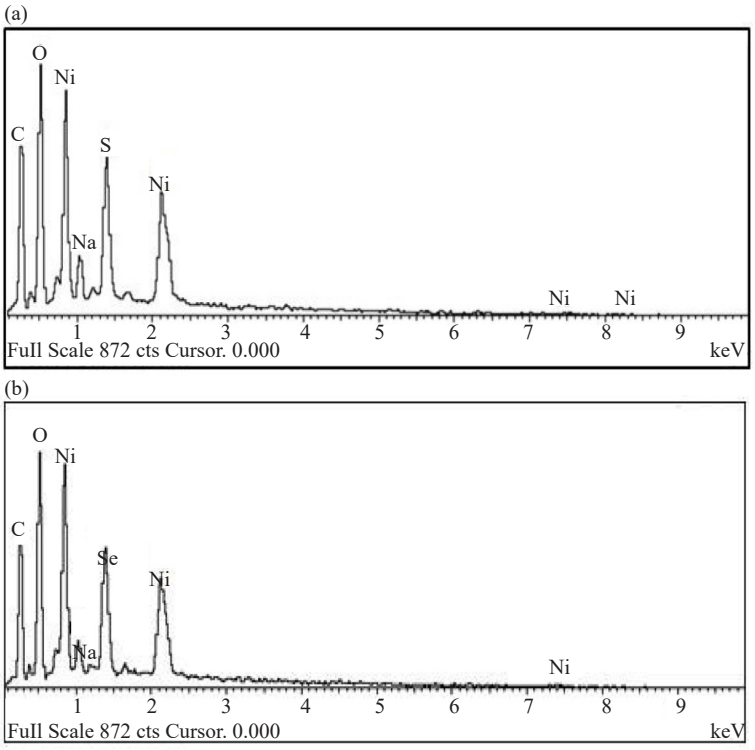

Figure 7. EDX spectrum of electrodeposited films at 30 minutes (a) $NiTe_2$ (b) $NiSe_2$

Table 2. Compositional study of NiX_2 (X = Te, Se) excluding other constituents

Material	Atomic weight % Ni: X (X = Te, Se)	Atomic ratio NiX_2 (X = Te, Se)
$NiTe_2$	32.74 : 64.33	NiTe 1.96
$NiSe_2$	31.48 : 62.45	NiSe 1.98

3.5 *Optical properties of electrodeposited thin films*

The optical absorption spectra of NiX_2 (X = Te, Se) thin films deposited onto ITO glass substrate was studied in the wavelength range 200-1,100 nm without considering losses due to reflection and transmission. Optical behavior of a material is vital for photoelectrochemical application and generally utilized to determine its optical constants, i.e. absorption coefficient (α), extinction coefficient (k), optical band gap (E_g) etc [40]. For this purpose, absorbance data, amount of light absorbed by the sample are taken.

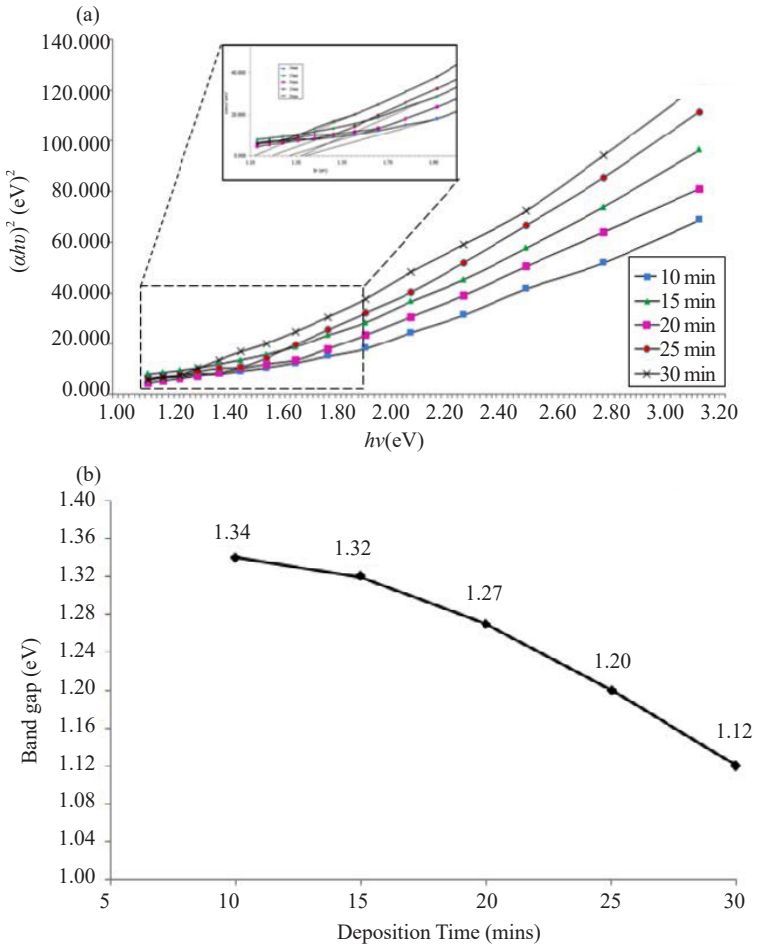

Figure 8. Variation of $NiTe_2$ thin films deposited at different deposition times (a) $(\alpha h\nu)^2$ vs. $h\nu$ and (b) bandgap vs. deposition time

From the optical absorbance versus wavelength data, band gap energy and band transition type was derived from mathematical treatment of the data with the following relationship for near-edge absorption [41].

$$A = [k(h\upsilon - E_g)^{n/2}]/h\upsilon;\ \upsilon = C/\lambda \quad (4)$$

where υ is the frequency, h is the Planck's constant, C is velocity of light, λ is the wavelength, k equals a constant while n carries the value of either 1 or 4. Tauc's plot has employed to plot the $(\alpha h\upsilon)^{1/2}$ graph. According to [42]. Tauc's plot is the plotting of $(\alpha h\upsilon)^{1/2}$ as a function of photon energy ($h\upsilon$) for different values of n (n = 1 and 4) [24]. It ensures the direct and it's allowed transmissions in the material if a straight line is obtained for n = 1, it indicates a direct electron transition between the states of the semiconductor, whereas, the transition is indirect is a straight line graph is obtained for n = 4. The straight line intercepts to the energy axis yields the optical band gap [31]. The graph of $(\alpha h\upsilon)^2$ versus photon energy is shown in Figure 8a and the related E_g vs deposition time is plotted in Figure 8b.

From the Figure 8, it can be understand that the band gap range for NiS_2 film prepared at various deposition time is in the range of 1.34-1.12 eV. The obtained band gap range is in good agreement with the value reported [41, 43]. Similar observation shown in Figures 9a and b of the band gap range for $NiSe_2$ film prepared at various deposition times is in the range of 1.30-1.15 eV. The obtained band gap range is in good agreement with the value reported [44-45].

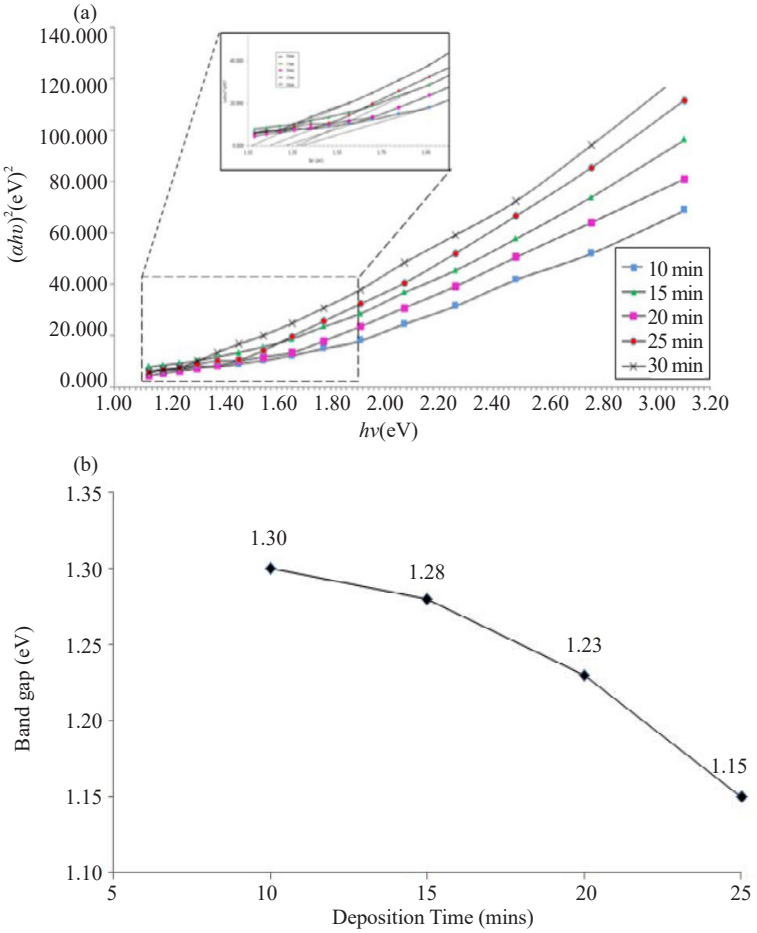

Figure 9. Variation of $NiSe_2$ thin films deposited at different deposition times (a) $(\alpha h\upsilon)^2$ vs. $h\upsilon$ and (b) bandgap vs. deposition time

These NiX_2 films optical band gap value is in the decrement trend that fits into the trend of thin film band gap values. It is observed that the values of these chalcogens are within the close range. It can be concluded that the optical bandgap energy of all types of films decreases as the deposition time of the film increases. This result correlates to film thickness, whereby an increase in deposition time of the films result in higher thickness which correlated as film thickness increases with respect to the amount of light energy [46]. When the deposition conditions like substrate

temperature of the film and solution concentration are kept fixed, the value of the band gap in general changes according to the thickness. According to Guneri et al., the reasons for this change can be one of the following: (i) largeness of the dislocation, (ii) quantum size effect (not relevant for thin film studies), (iii) changing barrier height due to variation in grain size in the polycrystalline film [35]. As it is evident that the band gap is affected by causing an alteration in the values of these band gap of the deposited films and decrease in barrier height is caused by an increase in grain size which in turn caused by an increase in film thickness. The decrease in energy band gap after long periods of deposition time is also attributed by improved crystallinity with sufficient thickness as supported by an increase in film thickness. The corresponding values of the band gap energy of the films with respect to film thickness are given in Table 3, is also reported that band gap decrease due to reduced Urbach energy in the optical band with increased film thickness. It is a good sign indicating decrease of defects in the film which is correlated to the disorder in the film [32].

Table 3. Bandgap energy values corresponding to film thickness of $NiTe_2$ and $NiSe_2$ thin films

Deposition time (mins)	$NiTe_2$		$NiSe_2$	
	Film thickness (μm)	Bandgap (eV)	Film thickness (μm)	Bandgap (eV)
10	0.8105	1.34	0.8641	1.30
15	0.8674	1.32	0.9222	1.28
20	0.9444	1.27	0.9846	1.23
25	1.0642	1.20	1.0864	1.15
30	1.1498	1.12	Film peeled OFF	

Overall, the time dependent parameters that effect the band gap are expected due to reorganization of the film and self-oxidation of the film which is apparent in SEM studies. By filling the voids in the film as the deposition time increases, denser films and smaller energy gap is expected.

4. Conclusion

Results proved that NiX_2 (X = Te, Se) thin films were successfully deposited on ITO-coated glass substrates. All films obtained were well adherent to the substrate with the help of TEA by adopting 'ion-by-ion' growth mechanism. The presence of TEA in basic condition results in the stoichiometric films with black-coloured, well-distributed and good adhesion films, enabling the optimum solar energy absorption. XRD analysis of the films proved NiX_2 (X = Te, Se) thin films is polycrystalline while EDX pattern confirmed the Nickle (Ni), Telluride (Te) and Selenium (Se) element presents in the thin film formed through electrodeposition process. Electron microscope analysis confirmed the uniform and smooth nature of the films. Optical studies show the direct optical bandgap energy of the film. Results on the semiconductor parameters of the films revealed it is of p-type material and all semiconductor values come in the range of many other transition metal chalcogenides and this has proven that NiX_2 (X = Te, Se) thin films is capable as a solar/PEC cell material.

Acknowledgement

The work presented in this manuscript was supported by the Ministry of Higher Education (MoHE), sponsored by KeTTHA/FRGS grant (Project No. FRGS/2011/FKP/TK02/1 F00120) and Universiti Teknikal Malaysia Melaka (UTeM).

Conflict of interest

The authors declare no competing financial interest.

References

[1] Hennayaka HMMN, Lee HS. Structural and optical properties of ZnS thin film grown by pulsed electrodeposition. *Thin Solid Films*. 2013; 548: 86-90.

[2] Haiyan Y, Xingwu G, Birbilis N, Wu G, Ding W. Tailoring nickel coatings via electrodeposition from a eutectic-based ionic liquid doped with nicotinic acid. *Applied Surface Science*. 2011; 257(21): 9094-9102.

[3] Yadav AA, Masumdar EU. Photoelectrochemical performances of n-$CdS_{1-x}Se_x$ thin films prepared by spray pyrolysis technique. *Solar Energy.* 2010; 84: 1445-1452.

[4] Anoud A, Halim MM, Yam FK, Al-Hardan NHM, Kaus NHM, Umar K, et al. The effect of substrate temperatures on the structural and conversion of thin films of reduced graphene oxide. *Physica B: Condensed Matter*. 2019; 572: 296-301.

[5] Duchatelet A, Sidali T, Loones N, Savidand G, Chassaing E, Lincot A. 12.4% Efficient Cu(In, Ga)Se_2 solar cell prepared from one step electrodeposited Cu-In-Ga oxide precursor layer. *Solar Energy Materials and Solar Cells.* 2013; 119: 241-245.

[6] Anand TJS, Shariza S. A study on molybdenum sulphoselenide (MoS_xSe_{2-x}, $0 \leq x \leq 2$) thin films: Growth from solution and its properties. *Electrochimica Acta.* 2012; 81: 64-73.

[7] Yadav AA, Masumdar EU. Photoelectrochemical investigations of cadmium sulphide (CdS) thin film electrodes prepared by spray pyrolysis. *Journal of Alloys and Compounds*. 2011; 509(17): 5394-5399.

[8] Hankare PP, Jadhav BV, Chate PA, Sathe DJ, Mulla IS. Synthesis and characterization of chemically deposited nickel substituted CdSe thin film. *Journal of Alloys and Compounds*. 2011; 509(6): 2948-2951.

[9] Luque PA, Quevedo-Lopez MA, Olivas A. Influence of deposition time on ZnS thin film growth over SiO_2 and glass substrates. *Materials Letters*. 2013; 106: 49-51.

[10] Jain P, Arun P. Influence of grain size on the band-gap of annealed SnS thin films. *Thin Solid Films.* 2013; 548: 241-246.

[11] Umar K, Haque MM, Mir NA, Muneer M, Farooqi IH. Titanium dioxide-mediated photocatalysed mineralization of two selected organic pollutants in aqueous suspensions. *Journal of Advanced Oxidation Technologies*. 2013; 16(2): 252-260.

[12] Rmili A, Ouachtari F, Bouaoud A, Louardi A, Chtouki T, Elidrissi B, et al. Structural, optical and electrical properties of Ni-doped CdS thin films prepared by spray pyrolysis. *Journal of Alloys and Compounds*. 2013; 557: 53-59.

[13] Sultana S, Rafiuddin, Khan MZ, Umar K, Ahmed AS, Shahadat M. SnO_2-SrO based nanocomposites and their photocatalytic activity for the treatment of organic pollutants. *Journal of Molecular Structure*. 2015; 1098: 393-399.

[14] Volobujeva O, Altosaar M, Raudoja J, Mellikov E, Grossberg M, Kaupmees L, et al. SEM analysis and selenization of Cu-In alloy films produced by co-sputtering of metals. *Solar Energy Materials and Solar Cells.* 2009; 93(1): 11-14.

[15] Pramanik P, Biswas S. Deposition of nickel chalcogenide thin films by solution growth techniques. *Journal of Solid State Chemistry*. 1986; 65(1): 145-147.

[16] Umar K, Aris A, Ahmad H, Parveen T, Jaafar J, Majid ZA, et al. Synthesis of visible light active doped TiO_2 for the degradation of organic pollutants-methylene blue and glyphosate. *Journal of Analtical Science and Technology.* 2016; 7: 29.

[17] O'Brien P, Park JH, Waters J. A single source approach to deposition of nickel sulfide thin films by LP-MOCVD. *Thin Solid Films.* 2003; 431-432: 502-505.

[18] Zhuang Z, Peng Q, Zhuang J, Wang X, Li Y. Controlled hydrothermal synthesis and structural characterization of a nickel selenide series. *Chemistry-A European Journal*. 2005; 12(1): 211-217.

[19] Hankare PP, Jadhav BV, Garadkar KM, Chate PA, Mulla IS, Delekar SD. Synthesis and characterization of nickel selenide thin films deposited by chemical method. *Journal of Alloys and Compounds*. 2010; 490(1-2): 228-231.

[20] Buhl J-C, Schuster K, Robben, L. Nanocrystalline sodalite grown from superalkaline NaCl bearing gels at low temperature (333K) and the influence of TEA on crystallization process. *Microporous and Mesoporous Materials*. 2011; 142: 666-671.

[21] Mahalingam T, Thanikaikarasan S, Dhanasekaran V, Mariappan R, Jayamurugan P, Velumani S, et al. Electrochemical deposition and studies on $CdCr_2S_4$ thin films. *Materials Science and Engineering: B*. 2010; 174(1-3): 249-252.

[22] Yadav AA. Effect of Fe-incorporation on photovoltaic characteristics of nano-structured CdSe thin films. *Journal*

of Alloys and Compounds. 2013; 552: 318-323.
[23] Wang C-H, Cheng K-W, Tseng C-J. Photoelectrochemical properties of $AgInS_2$ thin films prepared using electrodeposition. *Solar Energy Materials and Solar Cells.* 2011; 95: 453-461.
[24] Anand TJS, Zaidan M. Electro synthesised $NiTe_2$ thin films with the influence of additives. *Advanced Materials Research*. 2014; 925: 159-163.
[25] Zainal Z, Saravanan N, Mien HL. Electrodeposition of nickel selenide thin films in the presence of triethanolamine as a complexing agent. *Journal of Materials Science: Materials in Electronics*. 2005; 16: 111-117.
[26] Dhanasekaran V, Mahalingam T, Chandramohan R, Rhee J-K, Chu JP. Electrochemical deposition and characterization of cupric oxide thin films. *Thin Solid Films.* 2012; 520(21): 6608-6613.
[27] Sobhani A, Salavati-Niasari M. Synthesis and characterization of a nickel selenide series via a hydrothermal process. *Superlattices and Microstructures*. 2014; 65: 79-90.
[28] Dukstiene N, Kazancev K, Prosicevas I, Guobiene A. Electrodeposition of Mo-Se thin films from a sulfamatic electrolyte. *Journal of Solid State Electrochemistry*. 2004; 8: 330-336.
[29] Toma O, Iftimie S, Besleaga C, Mitran TL, Ghenescu V, Porumb O, et al. New investigations applied on cadmium sulfide thin films for photovoltaic applications. *Chalcogenide Letters*. 2011; 8(12): 747-756.
[30] JCPDS file number 003-0734.
[31] JCPDS file number 018-0886.
[32] Joseph Sahaya Anand T, Shariza S, Rosli ZM, Azizah S, Sivarao S, Mohamad RS, et al. Optical and Mott-Schottky studies of ternary MoSSe thin films synthesized by electrochemical route. *World Applied Sciences Journal*. 2013; 21: 60-67.
[33] Benramache S, Ben H, Arif A, Guettaf A. Correlation between the structural and optical properties of Co doped ZnO thin films prepared at different film thickness. *Optik-International Journal for Light and Electron Optics.* 2014; 125: 1816-1820.
[34] Ikhmayies SJ. The influence of the substrate temperature on the properties of solar cell related thin films. In: Kolesnikov N. (Ed.) *Modern Aspects of Bulk Crystal and Thin Film Preparation*. Croatia: InTech; 2012. p.337-356.
[35] Usha RP, Oommen R, Sanjeeviraja C. Improved photoelectrochemical performance of $(Bi_{1-x}Sb_x)_2S_3$ photoanodes. *Thin Solid Films.* 2013; 531: 76-80.
[36] Guneri E, Ulutas C, Kirmizigul F, Altindemir G, Gode F, Gumus C. Effect of deposition time on structural, electrical, and optical properties of SnS thin films deposited by chemical bath deposition. *Applied Surface Science*. 2010; 257(4): 1189-1195.
[37] Anand TJS. Synthesis and characterization of MoS_2 films for PEC cells. *Sains Malaysiana*. 2009; 38(1): 85-89.
[38] Alvi MA. Influence of thermal annealing on optical constants of Ag doped Ga-Se chalcogenide thin films. *Optics Communications.* 2013; 295: 21-25.
[39] Anuar K, Zulkarnain Z, Saravanan N, Zuriyatina A, Sharin R. Preparation and studies of nickel sulfide thin films in the presence of sodium tartrate as a complexing agent. *Materials Science*. 2004; 10(2): 157-161.
[40] Xue J, Shen Q, Liang W, Liu X, Bian L, Xu B. Preparation and formation mechanism of smooth and uniform Cu_2O thin films by electrodeposition method. *Surface and Coatings Technology*. 2013; 216: 166-171.
[41] Zhou L, Tang N, Wu S, Hu X, Xue Y. Influence of deposition time on ZnS thin films performance with chemical bath deposition. *Physics Procedia.* 2011; 22: 354-359.
[42] Verma V, Katiyar M. Effect of the deposition parameters on the structural and magnetic properties of pulsed laser ablated NiO thin films. *Thin Solid Films.* 2013; 527: 369-376.
[43] Chui Y, Zuo S, Jiang J, Yuan S, Chu J. Synthesis and characterization of co-electroplated Cu_2ZnSnS_4 thin films as potential photovoltaic material. *Solar Energy Materials and Solar Cells.* 2011; 95(8): 2136-2140.
[44] Anuar K, Tan WT, Saravanan N, Ho SM, Teo D. Chemical bath deposition of nickel sulphide (Ni_4S_3) thin films. *Leonardo Journal of Sciences*. 2010; 16: 1-12.
[45] Anuar K, Tan WT, Abdullah AH, Jelas HM. Chemical bath deposition of NiSe thin films from alkaline solutions using triethanolamine as complexing agent. *Oriental Journal of Chemistry*. 2009; 25(4): 813-816.
[46] Anand TJS, Zaidan M, Shariza S. Effect of additives on optical measurements of $NiSe_2$ thin films. *Procedia Engineering*. 2013; 53: 555-561.
[47] Todorov R, Paneva A, Petkov K. Optical characterization of thin chalcogenide films by multiple-angle-of-incidence ellipsometry. *Thin Solid Films.* 2010; 518(12): 3280-3288.